NEUROMORPHIC
Computing and Engineering

PAPER

# Long-term potentiation mechanism of biological postsynaptic activity in neuro-inspired halide perovskite memristors

**Enrique Hernández-Balaguera**[1,2,*], **Laura Munoz-Díaz**[1], **Agustín Bou**[2], **Beatriz Romero**[1], **Baurzhan Ilyassov**[3], **Antonio Guerrero**[2,*] and **Juan Bisquert**[2,*]

[1] Escuela Superior de Ciencias Experimentales y Tecnología (ESCET), Universidad Rey Juan Carlos, 28933 Móstoles, Madrid, Spain
[2] Institute of Advanced Materials (INAM), Universitat Jaume I, 12006 Castelló, Spain
[3] Astana IT University, Mangilik El EXPO C1, 010000 Nur-Sultan, Kazakhstan
[*] Authors to whom any correspondence should be addressed.

**E-mail:** enrique.hernandez@urjc.es, aguerrer@uji.es and bisquert@uji.es

**Keywords:** halide perovskite, potentiation, synapse

OPEN ACCESS

RECEIVED
13 January 2023

REVISED
7 April 2023

ACCEPTED FOR PUBLICATION
20 April 2023

PUBLISHED
26 May 2023



## Abstract

Perovskite memristors have emerged as leading contenders in brain-inspired neuromorphic electronics. Although these devices have been shown to accurately reproduce synaptic dynamics, they pose challenges for in-depth understanding of the underlying nonlinear phenomena. Potentiation effects on the electrical conductance of memristive devices have attracted increasing attention from the emerging neuromorphic community, demanding adequate interpretation. Here, we propose a detailed interpretation of the temporal dynamics of potentiation based on nonlinear electrical circuits that can be validated by impedance spectroscopy. The fundamental observation is that the current in a capacitor decreases with time; conversely, for an inductor, it increases with time. There is no electromagnetic effect in a halide perovskite memristor, but ionic-electronic coupling creates a chemical inductor effect that lies behind the potentiation property. Therefore, we show that beyond negative transients, the accumulation of mobile ions and the eventual penetration into the charge-transport layers constitute a bioelectrical memory feature that is the key to long-term synaptic enhancement. A quantitative dynamical electrical model formed by nonlinear differential equations explains the memory-based ionic effects to inductive phenomena associated with the slow and delayed currents, invisible during the 'off mode' of the presynaptic spike-based stimuli. Our work opens a new pathway for the rational development of material mimesis of neural communications across synapses, particularly the learning and memory functions in the human brain, through a Hodgkin–Huxley-style biophysical model.

## 1. Introduction

Neuromorphic computing must continue to take steps. The road ahead for the artificial neural networks, inspired by the human brain, consists of significantly advancing the understanding of the operational mechanisms of the nervous system (communications and functionalities) in order to develop reliable emerging circuits for memory applications [1]. One of the most complex structures to emulate in brain-like computation lays in the biological synapses which rely on the presence of ions and release of neurotransmitters that control the delay in the response [2]. This central process of learning, memory and inference in the cognitive human brain is indispensable for the real-time information-processing and transmission. Neuronal connections are highly sensitive to activity-induced patterns (synaptic plasticity) [3], strengthening, or weakening under high- or low-frequency stimulation, respectively. Both types of synapse-specific Hebbian forms of neuroplasticity, commonly known as long-term potentiation and depression [4, 5], underlie the ability of the brain to memorize and learn [4, 6], providing a basis for the development of artificial neurons and synapses. These changes of efficiency in synaptic transmission, depending on the spike timing [7, 8], have been the object of intensive research efforts during the past few years [9], with the aim, on the horizon, to develop phenomenological models in advanced neuroelectronic

materials that mimic the functions of biological neurons and synapses [10, 11]. In neuromorphic electronics, the essential synaptic behavior of potentiation has been recently observed in next-generation neuron-style perovskite memristors ascribed to an increasing conductance state of the device [12–16]. However, the origin of this ubiquitous and fascinating phenomenon has not been explained by using a biophysics-based electrical model, in the sense of Hodgkin–Huxley theory [17], that qualitatively explains the transient behavior and helps to articulate a consistent interpretation of the underlying ionic-electronic processes at different time scales.

In this work, we report a neuromorphic engineering approach to explore the origin of long-term potentiation systematically observed not only in the experimental transient responses under continuous pulsed operation of novel memristors that reproduce the postsynaptic currents, but also in photodetectors [18], light-emitting diodes [19, 20], and photoelectrochemical systems [21, 22]. Emerging perovskites have been used as model materials to create a neuromemristive device owing to the presence of activated ion migration channels. In recent and important applications of this technology, the research community has advanced in the understanding of how rich ionic dynamics affect device operation [23, 24]; however, further investigations are required to decipher the behavior of this material in the 'imitation game' of membranes in biological neurons. Here, ionic processes at the interfaces are the key to unraveling synaptic potentiation effects [25], which is one of the most important processes that trigger learning and memory fixation in the human brain. We analyze the high conduction state of perovskite memristors to a sequence of equally spaced impulses of constant areas in the range of high voltages, where the mechanism of inverted hysteresis emerges in the current–voltage characteristic [26]. In the initial responses, we observe the time transients, typically observed in resting conditions and caused by the 'conventional' ionic motion, in the current [27]. Nevertheless, for subsequent resulting currents in response to the pulse train excitation, the steady-state level (or the size of the synaptic component in the evoked response) persistently increases as an effect of the inherent memory dynamics of mobile ionic charges in perovskites, affecting to the dc conductivity. We present a nonlinear electrical model that reproduces the varying experimental current transients, discerning the underlying bioelectrical phenomena of this extraordinary process of synaptic functionality and making it possible to quantify the kinetic parameters that control the response in neuromorphic electronic devices through a consistent physical interpretation. Finally, we explore the results of the dynamic potentiation effects by regulating the frequency (in voltage) and changing the nature (current) of the applied stimuli. For verification purposes, impedance analysis was carried out over a wide range of voltages. These observations explain the electrical and material origins of the potentiation in synapsis-like memristors.

### 1.1. Transient and potentiation effects in synaptic devices

Figure 1 provides a summary of different types of artificial postsynaptic potentiation patterns. One of the most common ways to experimentally find this unique mechanism is given by a continuous increase of the resulting current, as shown in figure 1(a), in response to external voltage pulses that emulate presynaptic spikes [12]. This gradual increase in the electrical current can be also observed by applying consecutive voltage sweeps (refer to figure 1(b)) [15, 28], where the subsequent change in conductance, relatively similar to the synaptic potentiation of bio-synapses, is termed as 'analog switching process' in neuro-inspired memristor devices. These multilevel conductance states, which are essential for artificial synaptic applications, are not only visible with the repetition of voltage stimuli, but additional factors, such as the voltage range and operation time, lead to substantial changes in the current level of the device. An example of a perovskite memristor whose conductance changes at different scanning voltages is shown in figure 1(c) [13].

At this point, let us review the main types of transient responses, in response to a train of pulses, that are routinely observed in the study of artificial synapses and that we will analyze here. The ionic nature of perovskite memristors causes the intrinsic memory phenomena of potentiation, as evidenced by extraordinary complex transient responses, including ubiquitous spikes with changing trends, which lead to substantial increases in the current level and permanent resistive changes. As a relevant example, figure 1(d) shows the coexistence of the famous threshold switching mechanism and potentiation behavior in perovskite memristors, involving transient effects with 'multiple faces' that require an adequate framework of interpretation [13, 25, 29]. When sub-threshold voltages are applied, no potentiation effects are observable, as illustrated figure 1(d1). The current transients for all the trains of voltage pulses exhibit a relatively low initial peak and an ulterior decay with time because the device is still in the initial conduction state (static dynamics). However, the conductance is notoriously potentiated as the voltage goes up to higher values (dynamic behavior of the artificial synaptic devices). Intermediate voltage values cause negative spikes in the time transients, inverting the tendency of the standard decay processes (figure 1(d1)), thereby increasing the conductance levels and leading to slight potentiation mechanisms (refer to figure 1(d2)). Note that the transient current undershoots also increased gradually with the passage of the voltage pulses. Finally, the

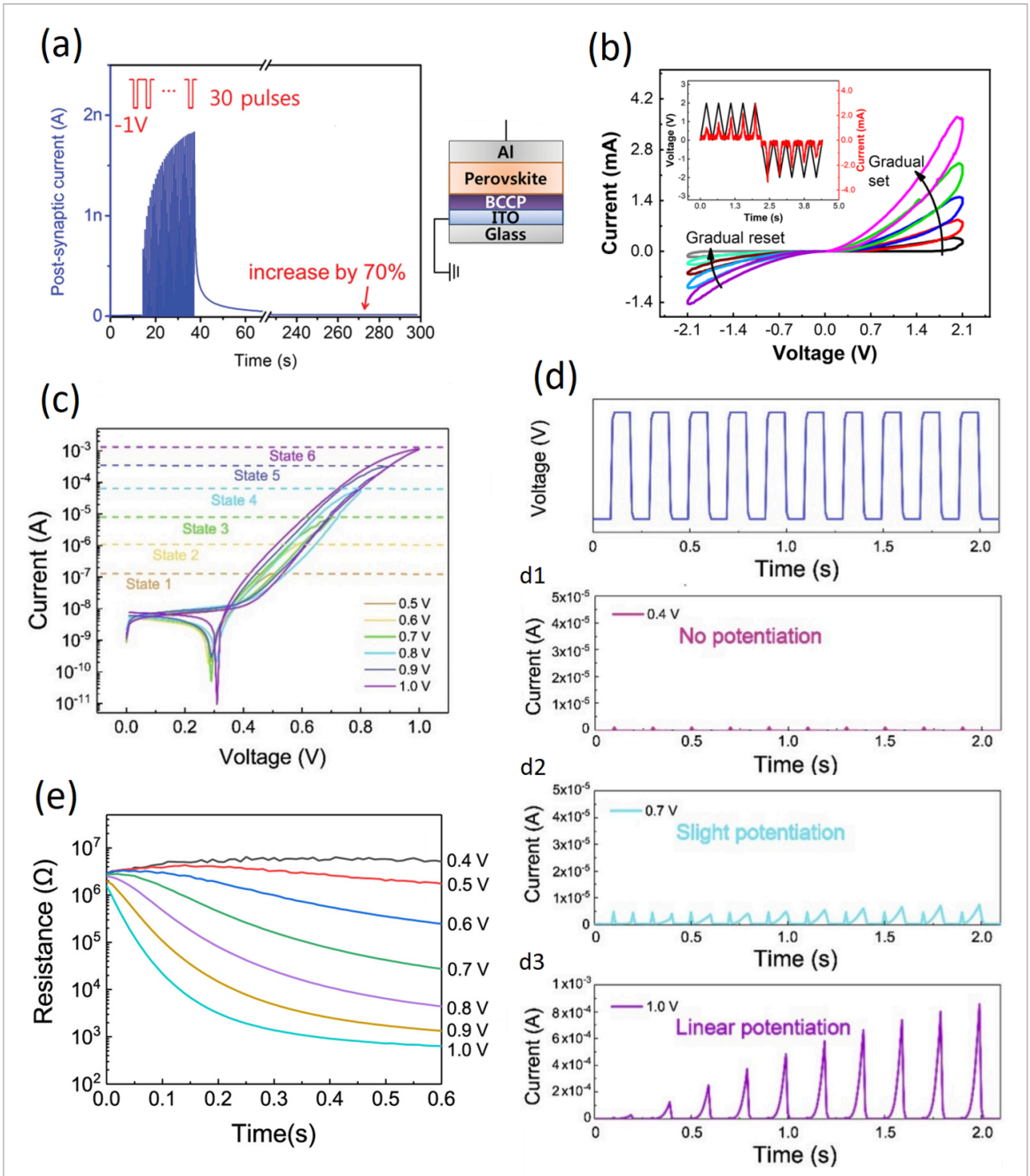


**Figure 1.** (a) Representative example of long-term potentiation achieved by application of consecutive rectangular pulses to the artificial synapse in a two-terminal perovskite-based memristor [12] John Wiley & Sons. [© 2016 WILEY-VCH Verlag GmbH & Co. KGaA, Weinheim]. (b) Experimental demonstration of potentiation and depression by repeating voltage sweeps in a general oxide-based memristor. Inset shows the device current response (red) to multiple subsequent voltammetries (black). Reproduced from [28]. CC BY 4.0. (c) Current–voltage curves with consecutively increased ranges that induced gradual setting processes in an organometal halide perovskite memristor. (d) Current responses of the memristor analyzed in (c) to rectangular pulse sequences with different amplitudes, leading from no potentiation (d1) at sufficiently low voltages to (d2) slight and (d3) significant artificial synaptic enhancement as the height of the pulses increases. (e) Subsequent variation of the conductance of the perovskite memristor with time. Reprinted from [13], Copyright (2020), with permission from Elsevier.

shape of the transient current responses shows an unusual type of behavior, different from the classical initial decays, in the extreme case of high-voltage excitations. As shown in figure 1(d3), the time transients exhibit dramatic and potentiated dynamics. Beyond this visual observation of the transient responses, a quantitative analysis requires the identification of the underlying bioelectrical mechanisms that cause this diversity of observed responses and, ultimately, to obtain a physical interpretation. Figure 1(e) summarizes the subsequent tendencies of the resistances over time as a function of voltage [13].

The waveform of the resulting responses previously explained in the scenario of high potentiation, in which the current increases slowly after an abrupt change in the voltage input, is a typical pattern found in a wide variety of memristors and related devices. Therefore, the model proposed here can explain a wide

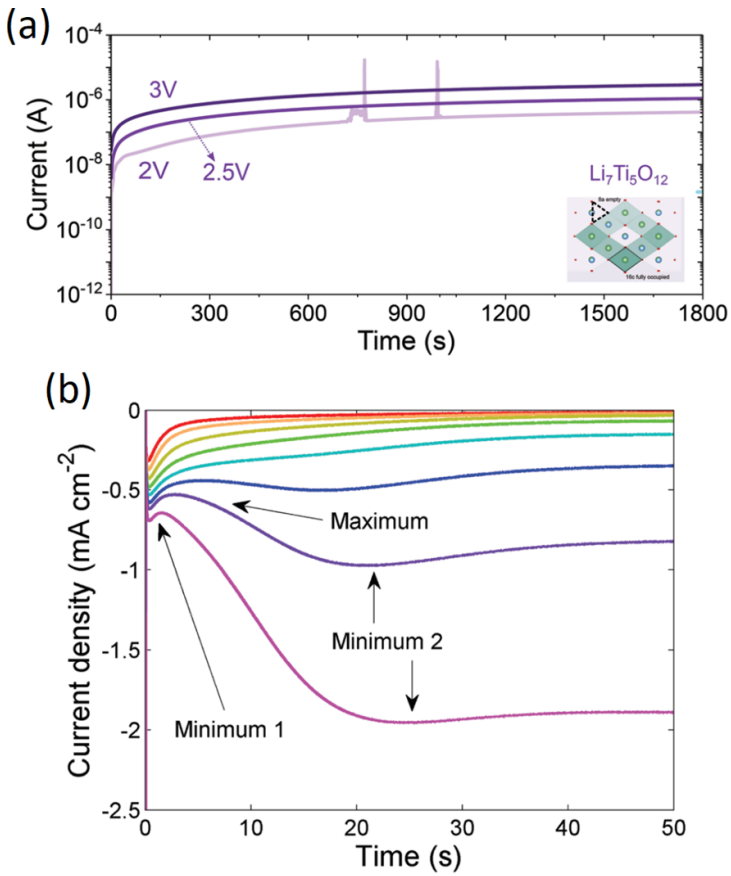


**Figure 2.** (a) Single-pulsing scheme of a neuro-inspired memristive Pt/$Li_7Ti_5O_{12}$/Pt device [30]. John Wiley & Sons. [© 2020 WILEY-VCH Verlag GmbH & Co. KGaA, Weinheim]. (b) Evolution of the experimental current density in a perovskite solar cell over 50 ms following a variable jump from different dc voltages in dark. Reproduced from [31]. CC BY 3.0.

variety of relaxation processes observed in the literature. Figure 2(a) shows the results of chronoamperometry experiments of a novel functional material based on lithium titanates (with a linear artificial neural training response in conductance) when the voltage increases, but now at high bias values and for long time spans. In this study [30], the authors interestingly demonstrated that the transient and potentiation mechanisms can be modulated by the original engineered lithiation state of the switching oxide. Again, we observed that the shapes of the waveforms were similar to those previously described. In effect, the transient and potentiation effects that we will explain here are commonly observed in classical oxide-based and novel memristor-based structures of memristors that mimic the functions of synapses with a high level of bio-fidelity. As a final and representative guide of the transient responses, figure 2(b) shows a similar correlation of the experimental current density evolution with the height of the applied step voltage in perovskite solar cells [31]. Here, authors suggest that the sign of the current depends on the ratio of generation to recombination mechanisms. Simulations based on drift-diffusion describe the dark current responses well, except for the negative spikes, which results in certain discrepancies. Therefore, it is plausible that the establishment of a consolidated framework of transient dynamics under single, repeated, and/or periodic stimuli is necessary because it has important implications for the understanding of potentiation operations in postsynaptic currents [12, 13], the design of biorealistic materials [11] and, more generally, for adequate modeling of a wide variety of electronic devices.

## 2. Results and discussion

### 2.1. Experimental visualization of synaptic potentiation operation

We examined a standard device with a memristor-based architecture consisting of glass/FTO/PEDOT:PSS (50 nm)/$MAPbI_3$ (500 nm)/Au (60 nm), containing both contacts that are selective to holes. To induce the ubiquitous effect of potentiation, we apply a train of voltage pulses of varying height, from 0.65 to 1.2 V (50% duty cycle), and frequency stimulation of 5 Hz in the dark. Note that the base-line voltage is 0 V (off mode in the pulse operation). Although the introduction of read voltages is a typical procedure to extract the conductance evolution with time in this type of studies focused on artificial synaptic plasticity [16, 32, 33],

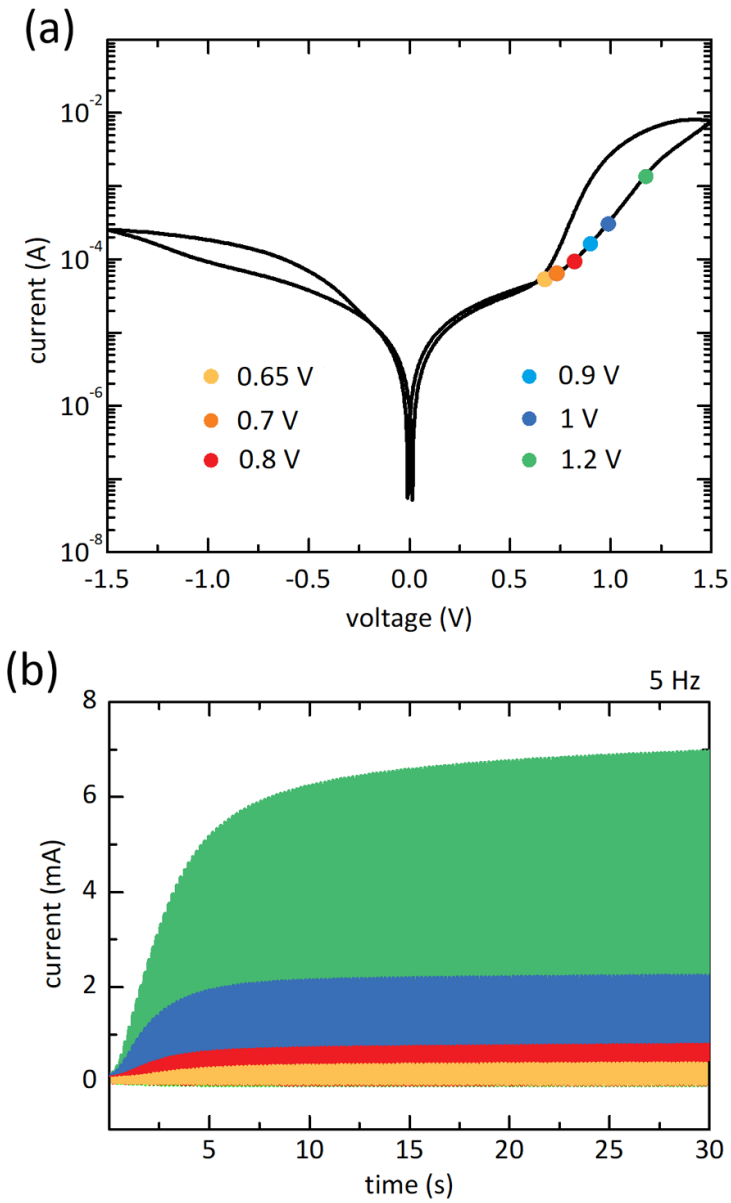


**Figure 3.** (a) Current–voltage response of the perovskite halide memristor measured at a scan rate value of 100 mV $s^{-1}$, with consecutively increased voltage steps (5 mV) that induce gradual setting and resetting mechanisms. (b) Transient currents in response to a train of rectangular pulses of some of the indicated voltage in (a)—from 0.65 to 1.2 V—and 5 Hz, demonstrating the long-term potentiation of the device's conductance.

we do not apply it here in order to facilitate the interpretation of time transient responses in terms of electrical models. We consider, in any case, that the potentiation effects can be evidenced through the current responses and, therefore, it is beyond the scope of this work. All preparation procedures and electrical measurements are described in detail in the methods section.

Figure 3(a) shows the current–voltage sweep characterization of our artificial synapse devices, indicating the precise values of the consecutive voltage pulses, mimicking the presynaptic spikes used in the time transient experiments. As can be seen in figure 3(b), the function of potentiation, emulating biological synapses, can be electrically activated and/or modulated in neuromorphic computing depending on the strength of the stimulus [13]. In effect, the current values, during the on mode in the pulse operation and just after turning off the voltage, increase and decrease, respectively, more dramatically with the application of larger amplitude pulses, as illustrated in figures 4(a) and (b). This potentiation effect of the resulting current has been amply observed in the literature, both in response to a train of voltage pulses [12–14, 29] and sweeping voltages [28] in neuro-inspired electronic devices, as noted above. Nevertheless, to the best of our knowledge, the electrical mechanisms behind this star synaptic function have not yet been elucidated.

For convenience, we extracted here very different transient current responses in the process of artificial synaptic potentiation at well-separated timescales. In the expanded view of the initial transient currents

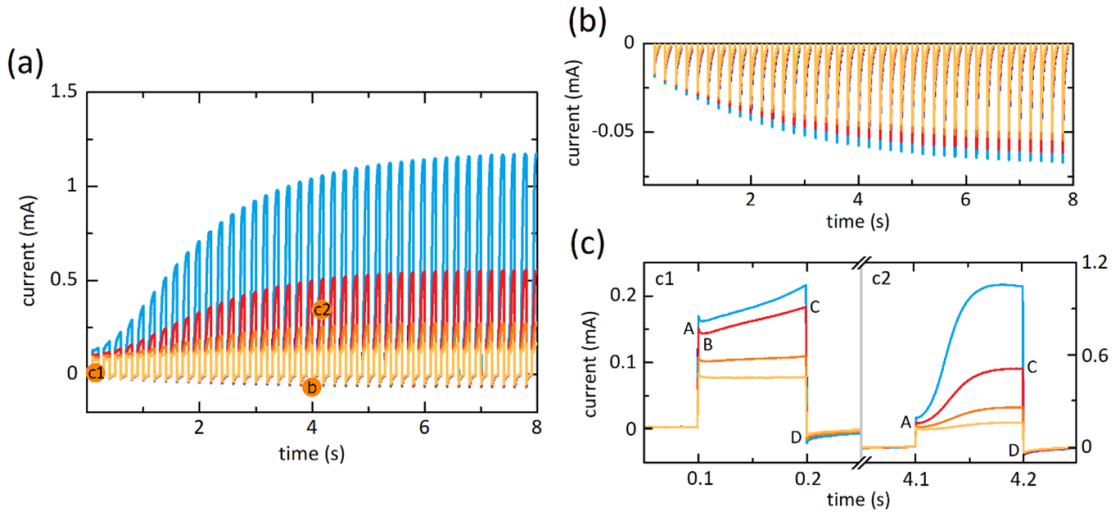


**Figure 4.** (a) Waveforms of the resulting currents in response to the initial part of the voltage pulse-train stimulus. For the sake of clarity, only time transients to the lower voltage excitations are shown here. (b) Expanded view of the negative discharge characteristics when the voltage is switched off. (c) Representative transition from classical negative transient spikes (c1), found in the initial part of the current response, to progressively enhanced inductive dynamics (c2), as an example of the artificial synaptic potentiation, obtained under the application of numerous voltage pulses.

(refer to the left panel of figure 4(c)), one can observe mixed dynamics, caused by the inherent competition, in the charge phase, between an interfacial charge accumulation effect (initial fast decay, from A to B) and a time-delayed redistribution ionic process (long tail or relatively slow rise, from B to C), with a negative overshoot (point B). From an electrical point of view, both effects can be correlated with the charge of the interfacial capacitance and slow non-electromagnetic inductor. Before we proceed any further, we should indicate that, in a previous paper [34], the authors obtained identical time transient responses to single-pulsing voltage perturbations, under certain conditions, by using a two-dimensional model and numerical simulations. Similarly, the dominant effect of the chemical inductor could be observed through the temporal evolution of the non-linear resistance in perovskite-based synaptic memristors, where the internal crossfire between charge trapping and ion migration also forms fascinating transient dynamics (with positive and negative spikes) that define the degree of artificial neuroplasticity [35].

When the pulse is switched off, the current swings negatively (point D); that is, the direction of the current is abruptly inverted, which leads us to consider the existence of bulk-resistance effects. The ulterior discharge characteristics, in comparison with the positive portions of the current, have no spikes, suggesting that there is no inductive feature at 0 V of applied voltage bias [36, 37]. This is the key point of artificial synaptic potentiation, which will be explained in detail later. Note that a more primitive stage can be found under relatively low voltage excitations, where the initial transients only show capacitive decays that evolve with the passage of the pulses to inductive dynamics, enhancing the conductance of the device.

Giant inductive effects, on the other hand, are revealed and become much more pronounced under continuous pulsed operation (refer to the right panel of figure 4(c)), originating from memory-based interfacial ionic phenomena, the fundamental basis of the origin of long-term synaptic potentiation. In effect, the current responses in this time window do not exhibit negative overshoots (point B disappears) because the interfacial capacitive effects lose relevance and thus vanish in the time transients. It is important to complete the exploration of figure 4(c) because, according to these views, the experimental time transient in figure 4(c2) shows a much more prominent change in the current, just after the step change at the trailing edge of the voltage pulse (from C to D), than that in figure 4(c1), which seems to be somehow connected with the same physical mechanism of the increasing inductive phenomena.

It should be mentioned that we have checked the cyclability and resistive-switching endurance of the perovskite memristors under a series of voltage sweeps and pulses. The conductance states and number of electrical pulses that one needs to apply to decrease the resistance of the devices were approximately the same as in the first measurement.

### 2.2. Dynamical model

Based on the observations of the current response to the pulsed voltage, it is necessary to propose an advanced model that tracks the transformation of transient dynamics from capacitive to inductive effects (both related to ionic-controlled interface recombination mechanisms) and, perhaps more importantly, has

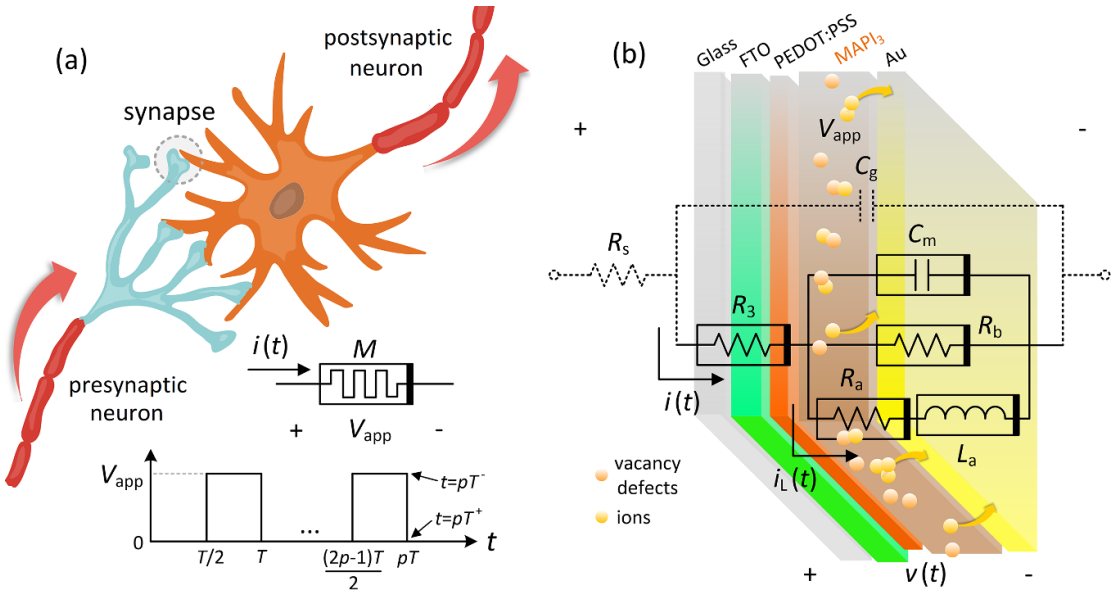


**Figure 5.** (a) Illustration of biological synapse and the electrical equivalent implementation to evidence long-term potentiation of postsynaptic activity, consisting of a memristor-based circuit model that receives voltage spikes in form of a train of rectangular pulses. (b) Schematic diagram of the general nonlinear equivalent circuit model underlying to the ionic-electronic phenomena that take place at the interfaces of a halide perovskite memristor, as a mirror version of biological neurons. The electrical model constitutes a simplified version of the complete circuit, ignoring, for example, the parasitic resistance, $R_s$, and the dielectric capacitance, $C_g$ (negligible in the recorded transient current responses).

the ability to remember the previous history (memory effects), retaining information when the voltage is switched off. As the starting point, we consider the representation of a voltage-controlled memristive device [38, 39] as shown in figure 5(a), adapted to obtain the general structure of a conduction-polarization system (including capacitive charging), as is the case here for the transient current–voltage behavior of halide perovskites with the memory effect [40].

The applied potential difference in the device is denoted $V_{app}$, the surface potential in the active interface as $v(t)$ and the current across the device as $i(t)$. At high voltages, this current is affected by an internal system-dependent process that includes the memory effect and leads to chemical inductive behavior. This abnormal mechanism is represented by a general and internal state variable $x(t)$ that undergoes a slowing down response (not instantaneous) by a voltage-driven adaptation function $g(x,v)$, to the external stimulus [40, 41]. The conduction channel of the conductivity function is represented by $f(v,x)$. Therefore, the memristive device can be described by the following generalization of nonlinear coupled dynamical equations in the scenario of high-voltage excitations:

$$i(t) = \frac{\mathrm{d}Q_S(v)}{\mathrm{d}t} + \frac{1}{R_M} f(v,x) \tag{1}$$

$$\tau_k \frac{\mathrm{d}x}{\mathrm{d}t} = g(x,v) \tag{2}$$

where $Q_S$ is the surface charging function, $R_M$ is the resistance scale parameter (for memory conductance), and $\tau_k$ is the slow characteristic time.

The general structure of equations (1) and (2) represents notorious two-dimensional dynamical neuron models in the style of the FitzHugh–Nagumo (FHN) equations, once the nonlinear functions $f(v,x)$ and $g(x,v)$ are defined to describe the specific properties of the phenomenon under study (here, long-term potentiation of synaptic activity) [42]. Equations (1) and (2) can be viewed as a memristive element [43, 44], capable of replicating the biological postsynaptic activity, which is connected to a pulsed voltage source, similar to presynaptic spikes, and the relaxation current is subsequently recorded under different stimulation amplitudes and frequencies. Figure 5(a) illustrates the experimental waveforms of the 'pulsing section' (of a generalized height, $V_{app}$) applied to the memristor. In our transient analysis, the charging processes are stopped at $t = pT$ (where $T$ is the duration of each cycle and $p$ denotes the pulse number, $p = 1, 2, 3\ldots$), when negative step transitions of the input occur and the current $i(t)$ has jump discontinuities.

We now introduce a bio-realistic long-term potentiation model for halide perovskite memristors. From an inspection of the observed transient responses (figure 4), it can be inferred that the current $i(t)$ can flow

along three flow paths: (i) charging the interfacial capacitance $C_m$, (ii) extracting a rapid current at the contacts (current $I_R(v)$), and/or (iii) slowly via an ion-modulated current, $i_L(t)$. This implies that $f(v,\ i_L) = I_R(v) + i_L(t)$. Here, the general conduction function is decoupled in an instantaneous current $I_R(v)$ interpreted as a recombination current, and a slow variable current $x = i_L(t)$ is delayed by a characteristic time $\tau_{LT}$ owing to slow ionic effects. On the other hand, the adaptation function is also separated to additive components as $g(v, i_L) = I_L(v) - i_L(t)$, where $I_L(v)$ represents the steady-state value of the internal recovery current that remains when the transient effect is over.

In summary, we obtain the following dynamical model in the style of neuronal models:

$$i(t) = \frac{dQ_S(v)}{dt} + I_R(v) + i_L(t) \tag{3}$$

$$\tau_{LT}\frac{di_L(t)}{dt} = I_L(v) - i_L(t). \tag{4}$$

The general structure of equations (3) and (4) is analogous to that of the FHN model [42, 45]. In the neuronal FHN theory, the instantaneous conductivity function $I_R(v)$ contains a negative resistance sector that leads to bifurcation and spiking [41]. In the case of the synaptic function described here, the functions $I_R(v)$ and $I_L(v)$ grow exponentially with the voltage, as detailed in the Methods section, corresponding to the established behavior of halide perovskite devices [46].

Figure 5(b) shows the proposed nonlinear equivalent circuit, valid for the analysis over a wide voltage range, of conductance potentiation dynamics, and the comprehension of the mechanisms that form these fascinating transient responses in perovskite memristors. Here, $C_m = {}^{dQ_S}/_{dv}$ is the surface capacitance; $R_3$, $R_b$, and $R_a$ are the variable resistances connected to $i\left(V_{app} - v\right)$ (i.e. the stationary value of the interfacial current, $i(t)$), $I_R(v)$, and $I_L(v)$, respectively; and $L_a$ is the chemical inductor associated with the delayed surface current. Indeed, this electrical model is not a 'normal circuit.' The applied voltage enormously changes the value of the elements, being interdependent among them [47]. In contrast, the conventional impedance measurements provide a summary vision of the elements, invariable for the value of the ac small signal voltages, which control the physical response and immediately give a meaningful content of the model [37]. The application of this technique is indeed a reasonable supporting point because, in this scenario, the equivalent circuit is linear (see below). The additional elements present in the circuit model are the geometric capacitance $C_g$ and the series resistance $R_s$ of the contacts.

### 2.3. Simulation of the potentiation process from the electrical circuit

We will now explore the dynamical behavior of our halide perovskite memristor model to evaluate synaptic efficacy modulation (transient current response to a voltage pulse-train stimulus) in terms of the self-sustained long-term potentiation that replicates very important mechanisms in the human brain. At this point, we aim to answer the crucial question: What is the reason for the gradual increase in the conductance of the device, which is relatively similar to the synaptic potentiation process in biological memory? To solve this question, we focused our attention on testing whether the dynamical behavior of the voltage-dependent chemical inductor, formed by time-delay ionic interactions [40], can explain the set of anomalous transient results observed here. For this purpose, we used the dynamical equations previously indicated, but particularized them to the key variables in the conductance potentiation process (see currents and voltages labeled in figure 5(b)). The details of the resolution of the nonlinear model are provided in the methods section.

In figure 6(a), we observe that our simulations reproduce the anomalous transient current behavior observed in the artificial synaptic functionality of the potentiation protocol (refer to figures 3(b) and 4(a)). At the leading edge of the pulses, when the input voltage undergoes positive step changes, $i(t)$ exhibits repetitive capacitive peaks because only ${}^{dQ_S(v)}/_{dt}$ has a non-zero value. Immediately after, the output current responds differently, depending on the number of preceding pulses. For instance, the initial transient responses with negative spikes during the on-time, approximately for $t < 1$ s, are explained by the clear transition from capacitive to inductive phenomena (or ionic-delayed interface recombination mechanisms) [27, 46]; in other words, the alternating dominance of the currents ${}^{dQ_S(v)}/_{dt}$ and $i_L(t)$ in $i(t)$, see equation (3). However, the displacement capacitive currents and the subsequent undershoots, with the passage of the voltage pulses (i.e. for $t > 1$ s), can be hardly identified or directly disappear, as can also be seen experimentally—refer to figure 4(a)–, owing to the impact of the previous steady state on the shape of the subsequent transient currents. In fact, theoretically speaking, the initial condition of $i_L(t)$ in equation (4) increases proportionally to the number of applied pulses due to the fact that the chemical inductor retains its charge, and hence its current, during the off mode in the pulse operation, because there is no way for such electrical element to discharge. Thus, the inductive mode of perovskite memristors, in the form of sharp

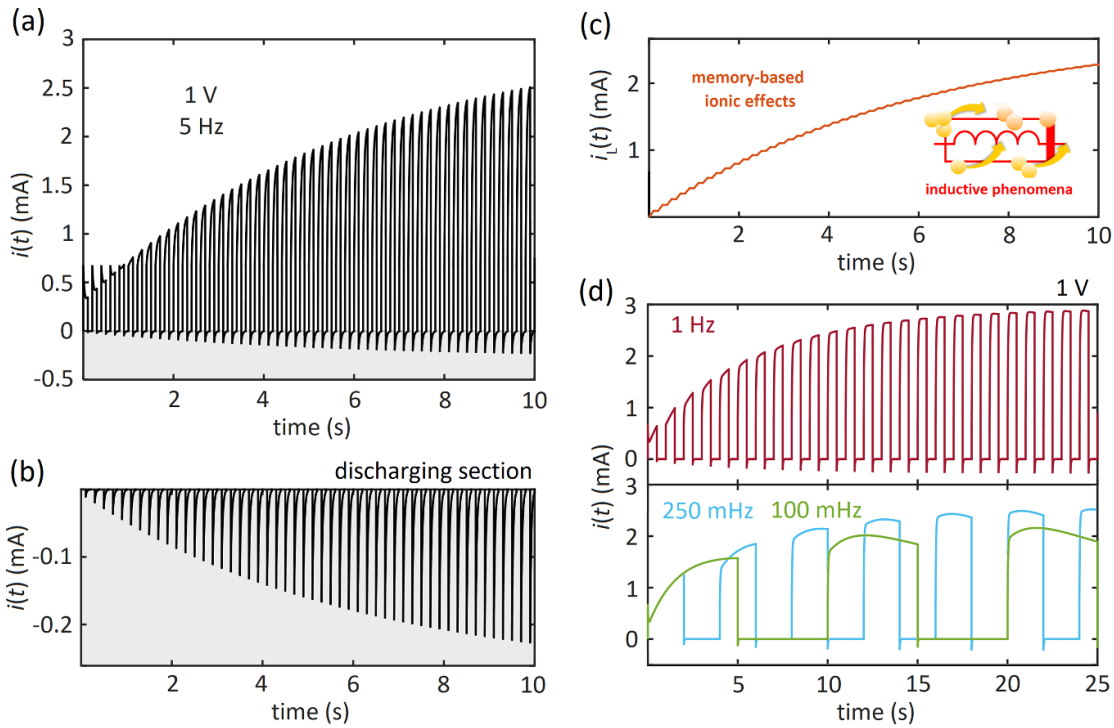


**Figure 6.** (a) Simulation of the transient current response to a train of uniformly spaced rectangular voltage pulses of 1 V and 5 Hz. (b) Inset of (a), where it is shown the trend in the values of the current just after the pulse is switched off, mimicking a spike-rate dependent plasticity learning rule. (c) Waveform of the simulated current response (or the slow memory-based function) flowing through the chemical inductor. (d) Current responses to voltage pulse sequences of 1 V with different frequencies, from 1 to 0.1 Hz, obtained from numerical computation.

rises, 'governs single handedly' the transient responses of the synaptic long-term potentiation, without capacitive decays and negative spikes. Equation (4) does not provide dynamism in the discharge phases, and is only visible to the capacitive processes. Note that the conduction current $I_R(v)$ manifests itself only when $dQ_S(v)/dt$ is relevant (for lower values of $i_L(pT)$). In summary, this complex and highly nonlinear effect constitutes a memory feature, and thus, a very interesting domain of study for interpreting the synaptic operation of any system through the general theory proposed here.

However, we show that our results provide experimental confirmation of the predictions by mimicking another example of spike-rate-dependent plasticity. In the case of our pulse stimulus, with a time interval of a few milliseconds, the effect on negative current, shown in the zoomed-in graph of figure 6(b), is reported, resulting in an enhancement of synaptic current [48]. The simulation results in negative discharge spikes that slightly decrease as the time increases, which is consistent with the experimental trend (*cf* Figure 4(b) and see methods section). Figure 6(c) shows the dynamic pattern of the internal variable $i_L(t)$ with a progressive increase during the on mode in the pulse operation, which promotes the long-term potentiation of the ion-channel conductance in the memristor-based neural network as a function of the voltage. When the driving voltage was turned off, $i_L(t)$ remained constant.

The physical origin of the activation and potentiation effects in memristors is currently under debate since several chemical and physical effects occur simultaneously [49]. One of the plausible explanations for neuro-inspired memristors relies on the slow response of mobile ions to the electrical field. While the voltage remains on iodide ions have time to respond and tend to accumulate at the perovskite/Au interface screening the electric field [19, 50] (related, theoretically, to a decrease of current) but, at the same time, leaving behind an increased number of halide vacancies in the perovskite that ultimately cause self-doping phenomena [25] and a consecutive enhancement in dc conductance—illustration of figure 5(b) [12]. In this way, halide vacancies form conducting channels or filamentary pathways that gradually growth in response to consecutive electrical stimulus, resulting in potentiation [16]. Indeed, some accumulated ions at the interface perovskite/Au, that have penetrated into the contact layer during the injection of voltage (and chemically interact with the reactive element), relax during the off mode in the pulse operation, involving these extra ion vacancy defects in the perovskite when the driving voltage is again turned on [19]: The 'game rules', in terms of the ionic landscape, change every time the pulse is switched on, potentiating here the effects of artificial synaptic transmission.

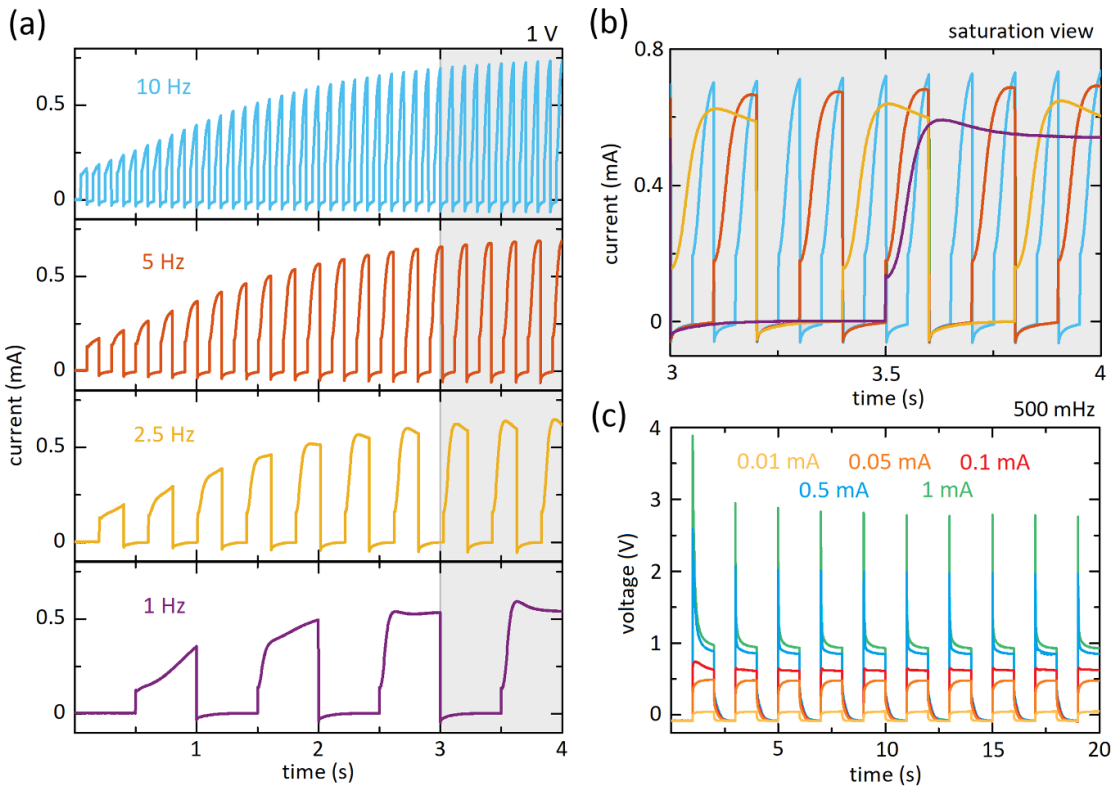


**Figure 7.** (a) Experimental comparison of the potentiation effect in device's conductance (transient-current response) as a function of stimulus frequency (voltage). An area of the saturation section is highlighted and zoomed in on (b). (c) Resulting transient voltages in response to a train of rectangular current pulses of variable height, from 10 $\mu$A to 1 mA, and 500 mHz, evidencing a clear static behavior in contrast of the dynamic effects obtained under voltage excitation.

Remarkably, when the numerical simulations were repeated but voltage impulse sequences of decreasing frequencies were applied, the shape of the waveforms was similar to that of current transients in the first stage of the pulse train, but with a less obvious conductance enhancement effect (see figure 6(d)) under the application of numerous voltage pulses. This differential characteristic is crucial for practical implementation of synaptic functions in an artificial neural network. In effect, these results show that the long-term potentiation is more easily saturable (lower current values) as frequency decreases, impairing the 'biological coupling' between the synaptic response and the firing of postsynaptic neurons [51]. To further prove the outlined theory, we next analyze, from an experimental perspective, the frequency-dependent potentiation effects.

### 2.4. Additional schemes of the memristor operation under pulse stimulation

For completeness, experimental measurements under low-frequency voltage stimulation were performed (figures 7(a) and (b)). From a physical point of view, the results showed that mobile ions driven by a slow electric field can more easily diffuse back to the initial position when low-frequency voltage signals are applied, leading to a less prominent conductance enhancement [13, 29]. In electrical terms, it seems that the value of the retaining current in the ionic inductor rapidly saturates, and the transient currents thus show intriguing waveforms with additional characteristics, consistent with our numerical simulations (figure 6(d)).

Another possible mechanism in the presence of ion migration was also investigated. In figure 7(c), we experimentally show that the potentiation process of memristor conductance cannot be manipulated by regulating the amplitude of the applied current stimulus. From our chronopotentiometric measurements, it is clear that the waveforms of the resulting transient voltages depend on the magnitude of the current excitation, similar to the voltage-controlled technique. At low currents, the results represent slight rounding of the pulse edges. Note that the edges are actually increasing exponential functions, that is, capacitive processes. Nevertheless, the voltage responses bear no resemblance to the pulse waveform at high current levels. They consist of initial spikes at the leading edge of the pulses and ulterior decays, which led us to consider the existence of slow inductive mechanisms. The main difference, in comparison with the previous scenario, is that the external current limits the memory pattern in ionic motion and thus constrains the current flowing through the chemical inductor during the off-time (different slow time constants), thereby

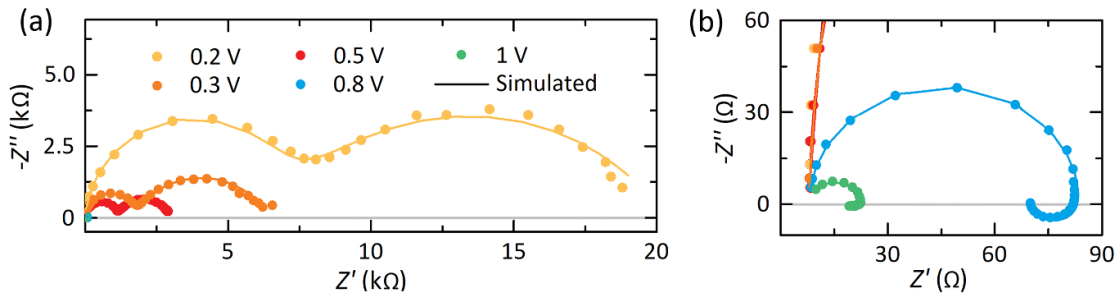


**Figure 8.** Complex plane plot representation of the impedance spectra obtained at (a) low and (b) high applied dc voltages, where the emerging negative capacitance effects are shown in a panel corresponding to a magnification of the scales.

preventing potentiation effects. In effect, the experimental results are consistent with our assumptions and can be easily deduced from the dynamic model previously described.

### 2.5. Impedance analysis

In the literature, the direct relation between the inverted hysteresis in the current–voltage curves and negative capacitance phenomena in perovskites, visualized at large voltage bias, has been widely demonstrated through inductive loops [36, 52] and negative transient spikes [27, 53] in the frequency and time domains, respectively. In this operational regime, just before the switching event, the conductance potentiation property emerges [28] coincide with inductive mechanisms in halide perovskite memristive devices. It is important to bear in mind this basic concept.

Although impedance spectroscopy is an experimental measurement subject to linear working conditions, it is now used to verify our results. A set of spectra for the perovskite memristors is shown in figure 8. At low voltages, the devices respond with a capacitive arc in the low-frequency region (figure 8(a)), while the inductive component is formed at high voltages, causing the famous negative capacitance effect [26, 54–56], which is visible in the zoomed-in view section shown in figure 8(b). Impedance data help to explain (i) the time-domain observations related to the overall experimental current waveforms in both the charge and discharge processes, (ii) the more evident potentiation of conductance under continuous pulsed operation as the voltage increases, and (iii) the inexistence of this unique effect at low voltages. These results corroborate our assumptions. However, it is necessary to emphasize that nonlinear problems, such as those studied here for artificial synaptic potentiation, have not been completely clarified using classical impedance analysis.

## 3. Conclusions

Interfacial phenomena in perovskite memristors mirror artificial versions of biological neuron processes. For this reason, obtaining an in-depth understanding of these brain-inspired devices can yield insights into overcoming the challenges faced by emerging neuromorphic computing and artificial intelligence.
Long-term potentiation is a critical synaptic feature in the learning and memory functions of the human brain, and we analyzed it in-depth to explain the origin of the nonlinear conductance properties of spiking neurons found in halide perovskite memristors. We investigated the potentiation effects of mimicked postsynaptic transient currents under pulse-mode voltage operation initially with varying periodic presynaptic spike amplitudes. Experimental transient measurements combined with electrical simulation of the device indicated that the memory effects of the time-delayed ionic redistribution were responsible for this fascinating phenomenon. Our dynamical electrical model explained that the change in the transient-current responses is due to the memory properties of a chemical inductive element (related to the delay effect), which is ‘accessible’ and thus charging during the on-time but ‘invisible’ and therefore retaining charge during the discharging phase. From a physical point of view, mobile ions change the internal electric field for each pulse, which leads to a more evident interface-controlled recombination, and thus, a change in neuron-style conductance states. In addition to analyzing the dominant role of the slow and delayed currents in artificial synaptic potentiation under relatively high-frequency voltage stimuli, our work also studies the resulting responses either when the frequency decreases or the nature of the excitation changes, with less (faster saturation, impairing synaptic enhancement) or no obvious potentiation mechanisms, respectively. This study determines the electrical origin of a unique transient behavior of synaptic operation in the human brain in the style of a Hodgkin–Huxley-type model devoid of bifurcations, paving the way for further

development of neural networks. In addition, it provides valuable information about the kinetic parameters that control the postsynaptic response and new understanding, especially when halide perovskites are used in pulsed operation (useful also for other important applications in different scientific communities, such as electrochemistry, electronics, and photovoltaics) and/or under steady-state conditions.

## 4. Methods

### 4.1. Device fabrication

All materials and solvents were used as received. fluorine doped tin oxide (FTO) glass (Pilkington TEC 15), PEDOT:PSS (Heraeus CLEVIOS™ P VP AI 4083), $CH_3NH_3I$ (methyl ammonium iodide (MAI), Greatcellsolar), $PbI_2$ (TCI, 99.99%), DMF (Sigma Aldrich, anhydrous 99.8%), (dimeyl sulfoxide DMSO (Sigma Aldrich, anhydrous 99.9%), chlorobenzene (Sigma Aldrich, 99.8%). The $MAPbI_3$ precursor solution was prepared using N,N-Dimethylformamide (DMF) solutions (50 wt%) containing MAI and $PbI_2$ (1:1 mol%) and MAI, $PbI_2$, and DMSO (1:1:1 mol%), as reported previously. Briefly, MAI (235 mg) and $PbI_2$ (681.5 mg) were mixed with DMF (1 ml) and Dimethyl sulfoxide (DMSO) (95 $\mu$l).

The devices were prepared according to previously reported methods. All the samples were prepared from FTO glass substrates. Etching was performed with zinc powder and HCl solution (2 M). Afterwards, the samples were brushed, cleaned with Hellmanex solution, and rinsed with Milli-Q water. For complete cleaning, the substrates were sonicated in acetone for 15 min, and this step was repeated using a mixed 50:50 ethanol-isopropanol solution. Finally, the substrates were dried with nitrogen and treated in a UV-$O_3$ chamber for 15 min. The PEDOT:PSS solution was filtered using a 0.45 $\mu$m syringe filter and spin-coated on the substrate at 3000 rpm for 30 s. This was followed by annealing at 120 Â °C for 10 min. The devices were transferred to a nitrogen-filled glovebox and the samples were heated at 100 °C for 5 min to avoid residual humidity on their surface. The perovskite precursor solution was spin-coated at 4000 rpm for 50 s using chlorobenzene as an antisolvent. Afterwards, the substrate was then annealed at 100 Â °C for 10 min. In the last step Au electrodes were thermally evaporated to define an active area of 0.25 $cm^2$ for measurements in the dark.

### 4.2. Electrical characterization

All electrical measurements were performed in a glove box filled with $N_2$. Dark current–voltage characteristics were recorded by performing cyclic voltammetry with a 5 mV step at a scan rate of 100 mV $s^{-1}$ using a PGSTAT204N potentiostat/galvanostat from Metrohm AutoLab. Note that the instrument was driven, for all electrical measurements, by the NOVA 2.1.5 software and, for this case, 10 *I–V* cycles were recorded starting in a forward direction from 0 V to 1.5 V, followed by a reverse direction from 1.5 V to −1.5 V, and finally recovered to 0 V. Under potentiostatic control, rectangular pulses of different heights, from 0.65 to 1.2 V, and durations of 0.05, 0.1, 0.2, and 0.5 s were applied into the memristive device. Note that the voltage level from which the pulses are initiated corresponds to 0 V. The current responses were recorded for 30 s, beginning at the instant the first pulse of the train was applied until the subsequent potentiation process was clearly visible. A sampling rate of 10 kHz was used, and all the experiments were repeated twice. We also checked the operation of the memristor under galvanostatic control, injecting rectangular pulses of different heights, of 0.01, 0.05, 0.1, 0.5, and 1 mA, and duration of 1 s and, subsequently, recording the voltage responses during 20 s. Impedance measurements were carried out using the AutoLab PGSTAT204N Potentiostat/Galvanostat (Eco-Chemie). Sinusoidal signals of 10 mV amplitudes were applied at 36 logarithmically spaced frequencies (five steps per decade) from 1 MHz to 100 mHz.

### 4.3. Numerical simulations

Our nonlinear electrical model was implemented to simulate the transient results using MATLAB's built-in ordinary differential equation solver based on the explicit formulae of Runge–Kutta (4,5) (ode45). Next, we provide details of our numerical simulations.

In the equivalent circuit of figure 5(b), the resistances exhibit exponential dependences on voltage, some of them correlated with the interfacial capacitance and/or chemical inductor, to obtain the unaltered impedance time constants, which are characteristic of perovskite devices [57]. Based on these assumptions, we write the exponential dependences in the currents in equilibrium conditions: $I\left(V_{\rm app}-v\right)=I_0 e^{\left(V_{\rm app}-v\right)/V_s}$, $I_{\rm R}\left(v\right)=I_{\rm R0}e^{v/V_s}$, and $I_{\rm L}\left(v\right)=I_{\rm L0}e^{v/V_b}$, where $I_0$, $I_{\rm R0}$, and $I_{\rm L0}$ are prefactors, and $V_s$ and $V_b$ are ideality factors with dimensions of voltage. Under stimulation ($(2p-1)\,T/2<t<pT$), the

model equation for the external current is

$$\tau_{ST}\frac{di(t)}{dt} = I_{R0}e^{v/V_s} - i(t) + i_L(t) \tag{5}$$

and for the slow memory variable:

$$\tau_{LT}\frac{di_L(t)}{dt} = I_{L0}e^{v/V_b} - i_L(t) \tag{6}$$

both obtained from Kirchhoff's laws, which are valid in nonlinear circuit models. Note that both the short- and long-timescale characteristic constants are defined as $\tau_{ST}(v) = R_3C_m$ and $\tau_{LT}(v) = {}^{L_a}/_{R_a}$ (see below). As $I\left(V_{app} - v\right) = I_R(v) + I_L(v)$ and $V_s \sim V_b$, the interfacial voltage $V$ in the steady state is given by

$$V = \frac{V_s}{2}\ln\left[\frac{I_0}{I_{R0} + I_{L0}}e^{V_{app}/V_s}\right]. \tag{7}$$

Thus, the bulk potential difference was obtained as $V_{app} - v$. From the linear approximation of the impedance, it is possible to determine the relationships of the voltage-dependent circuit elements: $R_3 = \left[{}^{dI}/_{d\left(V_{app} - v\right)}\right]^{-1} = \left({}^{V_s}/_{I_0}\right)e^{-\left(V_{app} - v\right)/V_s}$, $C_m = {}^{dQ_S}/_{dv} = C_{m0}e^{v/V_s}$, $R_b = \left[{}^{dI_R}/_{dv}\right]^{-1} = \left({}^{V_s}/_{I_{R0}}\right)e^{-v/V_s}$, $R_a = \left[{}^{dI_L}/_{dv}\right]^{-1} = \left({}^{V_b}/_{I_{L0}}\right)e^{-v/V_b}$, and $L_a = \tau_{LT}\left[{}^{dI_L}/_{dv}\right]^{-1}$. Therefore, the time constants are $\tau_{ST} = \left({}^{V_sC_{m0}}/_{I_0}\right)e^{\left(2v - V_{app}\right)/V_s}$ and $\tau_{LT} = \left({}^{V_sC_{m0}}/_{I_{R0}}\right)$, obtained, the last variable, through the property of nearly continuity of impedance characteristic times in perovskites, $\tau_{LT} = R_bC_m = {}^{L_a}/_{R_a}$ [37]. The model parameters, used in the simulations of figure 6, are: $I_0 = 0.66$ mA, $I_{R0} = 0.1$ mA, $I_{L0} = 1$ mA, $\tau_{ST} = 25$ ms, $\tau_{LT} = 3$ s, $V_s = 1$ V, and $V_b = 0.75$ V. Note that, for simplicity, we define an invariable short timescale characteristic constant that does not significantly affect the numerical simulations of potentiation.

Nevertheless, we assume that in the discharge phase, the current flowing through the chemical inductor $i_L(t)$ remains constant owing to memory effects (the resting time of duration is much shorter than the electrical inertia exhibited by the ionic charge redistribution, quantified through $\tau_{LT}(v)$). Mathematically, this is expressed as

$$i_L([2p-1]T/2) = i_L([p-1]T), \ (p-1)T < t < [2p-1]T/2. \tag{8}$$

The other initial condition is $i\left(\left[2p-1\right]{}^{T}/_{2}\right) = 0$ A. With the passage of the pulses (increasing values of $p$), the electrical current in the lower branch, considered just before the step changes from 0 to $V_{app}$, increases (i.e. the initial condition each time is longer), which affects the value of $R_a$, decreasing it, and thus increasing the steady-state conductance and current:

$$I = I_{R0}e^{v/V_s} + I_{L0}e^{v/V_b}. \tag{9}$$

Specifically, the values of the negative spikes when the step changes of the pulses occur (from $pT^-$ to $pT^+$) can be approximated by

$$i\left(pT^+\right) = -I_0e^{v\left(pT^-\right)/V_s}. \tag{10}$$

When the driving voltage is turned off, the current swings negatively by a variable amount, which leads to the existence of a nonlinear series resistance $R_3$. Then, it starts a pure exponential decay toward zero (with a larger slow time constant) in each half-cycle. However, the areas of the negative discharge characteristics above the zero axis are not approximately equal to those below the steady-state regime in the charging phase [34]. Obviously, these dynamical features of $i(t)$ involve different slow characteristic times as the charge processes. The current responses do not exhibit overshoots for $pT < t < (2p+1){}^{T}/_{2}$ because the ionic inductor is deactivated at low bias voltages [46]. Therefore, one can assume that the memory variable $i_L(t)$ is normally held constant and thus, equation (6) does not provide dynamism to the current response of the perovskite memristor in the discharge processes.

Figure 9 summarizes, from an electrical point of view, both the charging and discharging processes for $(2k-1){}^{T}/_{2} < t < kT$ and $kT < t < (2k+1){}^{T}/_{2}$, respectively, highlighting the inductive branch.

Impedance data were fitted to the linear version of the equivalent circuit shown in figure 5(b) using the ZView software.

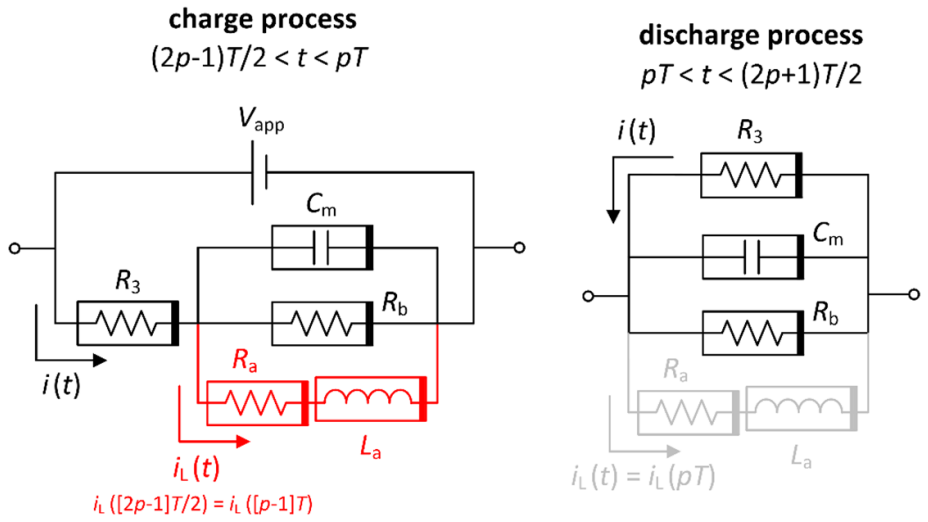


**Figure 9.** Equivalent circuits of figure 5(b) during the (a) on-time and (b) off-time.

## Data availability statement

The data that support the findings of this study are openly available at the following URL/DOI: https://doi.org/10.7910/DVN/7JOSNP.

## Acknowledgments

This work has received funding from the Comunidad de Madrid under the SINFOTON2-CM Research Program, S2018/NMT4326-SINFOTON2-CM, and the Universidad Rey Juan Carlos (Projects of Reference M2607 and M2993) via 'Research and development promotion Program'. We are grateful to Universidad Rey Juan Carlos (30. VC.IN.IN.541A.483.05) for the mobility funds granted. This study forms part of the Advanced Materials program and was supported by MCIN with funding from the European Union NextGenerationEU (PRTR-C17. I1) and Generalitat Valenciana.

## Conflict of interest

The authors have declared that no competing interests exist.

## ORCID iDs

Enrique Hernández-Balaguera https://orcid.org/0000-0002-1400-5916
Agustín Bou https://orcid.org/0000-0002-7535-5063
Baurzhan Ilyassov https://orcid.org/0000-0003-4563-2004
Antonio Guerrero https://orcid.org/0000-0001-8602-1248
Juan Bisquert https://orcid.org/0000-0003-4987-4887

## References

[1] Christensen D V *et al* 2022 2022 Roadmap on neuromorphic computing and engineering *Neuromorph. Comput. Eng.* **2** 022501
[2] Kandel E, Schwartz J H, Jessell T M, Siegelbaum S A and Hudspeth A J 2012 *Principles of Neural Science* (McGraw-Hill, Health Professions Division)
[3] Abbott L F and Nelson S B 2000 Synaptic plasticity: taming the beast *Nat. Neurosci.* **3** 1178–83
[4] Bliss T V, Collingridge G L and Synaptic A 1993 Model of memory: long-term potentiation in the hippocampus *Nature* **361** 31–39
[5] Linden D J and Connor J A 1995 Long-term synaptic depression *Annu. Rev. Neurosci.* **18** 319–57
[6] Whitlock J R, Heynen A J, Shuler M G and Bear M F 2006 Learning induces long-term potentiation in the hippocampus *Science* **313** 1093–7
[7] Song S, Miller K D and Abbott L F 2000 Competitive Hebbian learning through spike-timing-dependent synaptic plasticity *Nat. Neurosci.* **3** 919–26
[8] Wang H-X, Gerkin R C, Nauen D W and Bi G-Q 2005 Coactivation and timing-dependent integration of synaptic potentiation and depression *Nat. Neurosci.* **8** 187–93
[9] Malenka R C and Nicoll R A 1999 Long-term potentiation—a decade of progress? *Science* **285** 1870–4

[10] JoJo S H, Chang T, Ebong I, Bhadviya B B, Mazumder P and Lu W 2010 Nanoscale memristor device as synapse in neuromorphic systems *Nano Lett.* **10** 1297–391
[11] Wang Z *et al* 2017 Memristors with diffusive dynamics as synaptic emulators for neuromorphic computing *Nat. Mater.* **16** 101–8
[12] Xu W, Cho H, Kim Y-H, Kim Y-T, Wolf C, Park C-G and Lee T-W 2016 Organometal halide perovskite artificial synapses *Adv. Mater.* **28** 5916–22
[13] Yang J-Q, Wang R, Wang Z-P, Ma Q-Y, Mao J-Y, Ren Y, Yang X, Zhou Y and Han S-T 2020 Leaky integrate-and-fire neurons based on perovskite memristor for spiking neural networks *Nano Energy* **74** 104828
[14] Ham S, Choi S, Cho H, Na S-I and Wang G 2019 Photonic organolead halide perovskite artificial synapse capable of accelerated learning at low power inspired by dopamine-facilitated synaptic activity *Adv. Funct. Mater.* **29** 1806646
[15] Kim S J *et al* 2022 Vertically aligned two-dimensional halide perovskites for reliably operable artificial synapses *Mater. Today* **52** 19–30
[16] Kwak K J, Baek J H, Lee D E, Im I, Kim J, Kim S J, Lee Y J, Kim J Y and Jang H W 2022 Ambient stable all inorganic $CsCu_2I_3$ artificial synapses for neurocomputing *Nano Lett.* **22** 6010–7
[17] Hodgkin A L, Huxley A F and Quantitative A 1952 Description of membrane current and its application to conduction and excitation in nerve *J. Physiol.* **117** 500–44
[18] Ding J, Gao W, Gao L, Lu K, Liu Y, Sun J-L and Yan Q 2022 Unraveling the effect of halogen ion substitution on the noise of perovskite single-crystal photodetectors *J. Phys. Chem. Lett.* **13** 7831–7
[19] Kumawat N K, Tress W and Gao F 2021 Mobile ions determine the luminescence yield of perovskite light-emitting diodes under pulsed operation *Nat. Commun.* **12** 4899
[20] Sakhatskyi K *et al* 2022 Assessing the drawbacks and benefits of ion migration in lead halide perovskites *ACS Energy Lett.* **7** 3401–14
[21] Podborska A, Suchecki M, Mech K, Marzec M, Pilarczyk K and Szaciłowski K 2020 Light intensity-induced photocurrent switching effect *Nat. Commun.* **11** 854
[22] Hagfeldt A, Lindström H, Södergren S and Lindquist S-E 1995 Photoelectrochemical studies of colloidal $TiO_2$ films: the effect of oxygen studied by photocurrent transients *J. Electroanal. Chem.* **381** 39–46
[23] Eames C, Frost J M, Barnes P R F, O'Regan B C, Walsh A and Islam M S 2015 Ionic transport in hybrid lead iodide perovskite solar cells *Nat. Commun.* **6** 7497
[24] Meloni S *et al* 2016 Ionic polarization-induced current–voltage hysteresis in $CH_3NH_3PbX_3$ perovskite solar cells *Nat. Commun.* **7** 1–9
[25] Wang Y, Zhang Z, Xu M, Yang Y, Ma M, Li H, Pei J and Shi L 2019 Self-doping memristors with equivalently synaptic ion dynamics for neuromorphic computing *ACS Appl. Mater. Interfaces* **11** 24230
[26] Berruet M, Pérez-Martínez J C, Romero B, Gonzales C, Al-Mayouf A M, Guerrero A and Bisquert J 2022 Physical model for the current–voltage hysteresis and impedance of halide perovskite memristors *ACS Energy Lett.* **7** 124–1222
[27] Hernández-Balaguera E and Bisquert J 2022 Negative transient spikes in halide perovskites *ACS Energy Lett.* **7** 2602–10
[28] Ilyas N, Li D, Li C, Jiang X, Jiang Y and Li W 2020 Analog switching and artificial synaptic behavior of $Ag/SiO_x$: $Ag/TiO_x/P++$-simemristor device *Nanoscale Res. Lett.* **15** 30
[29] Das U, Sarkar P, Paul B and Roy A 2021 Halide perovskite two-terminal analog memristor capable of photo-activated synaptic weight modulation for neuromorphic computing *Appl. Phys. Lett.* **118** 182103
[30] Gonzalez-Rosillo J C, Balaish M, Hood Z D, Nadkarni N, Fraggedakis D, Kim K J, Mullin K M, Pfenninger R, Bazant M Z and Rupp J L M 2020 Lithium-battery anode gains additional functionality for neuromorphic computing through metal–insulator phase separation *Adv. Mater.* **32** 1907465
[31] O'Kane S E J *et al* 2017 Measurement and modelling of dark current decay transients in perovskite solar cells *J. Mater. Chem.* C **5** 452–62
[32] Li G *et al* 2022 Photo-induced non-volatile $VO_2$ phase transition for neuromorphic ultraviolet sensors *Nat. Commun.* **13** 1729
[33] Wang Y, Zheng Y, Gao J, Jin T, Li E, Lian X, Pan X, Han C, Chen H and Chen W 2021 Band-tailored van der Waals heterostructure for multilevel memory and artificial synapse *InfoMat* **3** 917–28
[34] Bisquert J and Guerrero A 2022 Dynamic instability and time domain response of a model halide perovskite memristor for artificial neurons *J. Phys. Chem. Lett.* **13** 3789–95
[35] Liu X *et al* 2022 Solution-processed synaptic memristors based on halide perovskite nanocrystals *J. Phys. Chem. Lett.* **13** 10994–1000
[36] Bisquert J, Guerrero A and Gonzales C 2021 Theory of hysteresis in halide perovskites by integration of the equivalent circuit *ACS Phys. Chem. Au* **1** 25–44
[37] Guerrero A, Bisquert J and Garcia-Belmonte G 2021 Impedance spectroscopy of metal halide perovskite solar cells from the perspective of equivalent circuits *Chem. Rev.* **121** 14430–84
[38] Pershin Y V and Di Ventra M 2011 Memory effects in complex materials and nanoscale systems *Adv. Phys.* **60** 145–227
[39] Chua L 2015 Everything you wish to know about memristors but are afraid to ask *Radioengineering* **24** 319–68
[40] Bisquert J and Guerrero A 2022 Chemical inductor *J. Am. Chem. Soc.* **144** 5996–6009
[41] Bisquert J 2022 Hopf bifurcations in electrochemical, neuronal, and semiconductor systems analysis by impedance spectroscopy *Appl. Phys. Rev.* **9** 011318
[42] Izhikevich E M 2007 *Dynamical Systems in Neuroscience* (Cambridge, MA: MIT Press)
[43] Chua L 1971 Memristor—the missing circuit element *IEEE Trans. Circuit Theory* **18** 507–19
[44] Strukov D B, Snider G S, Stewart D R and Williams R S 2008 The missing memristor found *Nature* **453** 80–83
[45] Bisquert J 2021 A frequency domain analysis of the excitability and bifurcations of the Fitzhugh–Nagumo neuron model *J. Phys. Chem. Lett.* **12** 11005–13
[46] Gonzales C, Guerrero A and Bisquert J 2022 Transition from capacitive to inductive hysteresis: a neuron-style model to correlate *I–V* curves to impedances of metal halide perovskites *J. Phys. Chem.* C **126** 13560–78
[47] Chua L, Desoer C A and Kuh E S 2000 *Linear and Non Linear Circuits* (McGraw-Hill Education)
[48] Rogdakis K, Loizos M, Viskadouros G and Kymakis E 2022 Memristive perovskite solar cells towards parallel solar energy harvesting and processing-in-memory computing *Mater. Adv.* **3** 7002–14
[49] Xiao X, Hu J, Tang S, Yan K, Gao B, Chen H and Zou D 2020 Recent advances in halide perovskite memristors: materials, structures, mechanisms, and applications *Adv. Mater. Technol.* **5** 1900914
[50] Tress W, Marinova N, Moehl T, Zakeeruddin S M, Nazeeruddin M K and Grätzel M 2015 Understanding the rate-dependent J–V hysteresis, slow time component, and aging in $CH_3NH_3PbI_3$ perovskite solar cells: the role of a compensated electric field *Energy Environ. Sci.* **8** 995–1004

[51] Bliss T V P and Lømo T 1973 Long-lasting potentiation of synaptic transmission in the dentate area of the anaesthetized rabbit following stimulation of the perforant path *J. Physiol.* **232** 331–56
[52] Alvarez A O, Arcas R, Aranda C A, Bethencourt L, Mas-Marzá E, Saliba M and Fabregat-Santiago F 2020 Negative capacitance and inverted hysteresis: matching features in perovskite solar cells *J. Phys. Chem. Lett.* **11** 8417–23
[53] Ebadi F, Taghavinia N, Mohammadpour R, Hagfeldt A and Tress W 2019 Origin of apparent light-enhanced and negative capacitance in perovskite solar cells *Nat. Commun.* **10** 1574
[54] Dualeh A, Moehl T, Tétreault N, Teuscher J, Gao P, Nazeeruddin M K and Grätzel M 2014 Impedance spectroscopic analysis of lead iodide perovskite-sensitized solid-state solar cells *ACS Nano* **8** 362–73
[55] Sanchez R S, Gonzalez-Pedro V, Lee J-W, Park N-G, Kang Y S, Mora-Sero I and Bisquert J 2014 Slow dynamic processes in lead halide perovskite solar cells. Characteristic times and hysteresis *J. Phys. Chem. Lett.* **5** 2357–63
[56] Fabregat-Santiago F, Kulbak M, Zohar A, Vallés-Pelarda M, Hodes G, Cahen D and Mora-Seró I 2017 Deleterious effect of negative capacitance on the performance of halide perovskite solar cells *ACS Energy Lett.* **2** 2007–13
[57] Zarazua I, Han G, Boix P P, Mhaisalkar S, Fabregat-Santiago F, Mora-Seró I, Bisquert J and Garcia-Belmonte G 2016 Surface recombination and collection efficiency in perovskite solar cells from impedance analysis *J. Phys. Chem. Lett.* **7** 5105–13